Egypt. J. Chem. **Vol. 68**, No. 5 pp. 419 - 430 (2025)

Egyptian Journal of Chemistry

http://ejchem.journals.ekb.eg/

Reduced Graphene/Cobalt Sulphide/ Titinum-Zirconiate for Dye-Sensitized Solar Cell

Doaa M. Atia[1*], Ninet M. Ahmed[1], Ali B. Abou Hammad[2], Marwa M. Toraya[1], Amany M. El Nahrawy[2]

[1]*Photovoltaic Cells Department, Electronics Research Institute, 11843, Cairo, Egypt*

[2]*Solid-State Physics Department, Physics Research Division, National Research Centre, 33 El-Bohouth St., Dokki, 12622, Egypt*

Abstract

Exploiting cost-effective Pt-free counter-electrode materials with low-cost synthesis and high catalytic activity is crucial for dye-sensitized solar cells. This paper introduces the sol-gel drop casting approach for preparing cobalt sulfide-doped graphene oxide (CoS/rGO). The cobalt sulfide-doped graphene nanocomposite exhibits electrocatalytic properties comparable to conventional Pt electrodes as the counter electrode (CE) in DSSCs. Cobalt sulfide-doped graphene nanocomposites were synthesized via a direct sol-gel approach as a low-cost substitute for Pt. Characterization using X-ray diffraction, scanning electron microscopy/energy-dispersive/transmission electron microscopy, and UV-Vis spectroscopy shows the successful formation of cobalt sulfide-doped graphene nanocomposites. The band gap energy of cobalt sulfide-doped graphene is 3.05 eV, which is lower than rGO (3.252 eV), due to enhanced light absorption in the visible range imparted by rGO. The open circuit voltage is 0.75 V, the short circuit current density is 17.88 mA/cm^2, and the fill factor is 0.527. Under the illumination of AM 1.5 simulated solar light (100 mW cm^{-2}), the DSSC based on the proposed CoS/rGO CE achieved an efficiency of 7.0759 %.

Keywords: Counter electrode; Pt-free; Photo-anode; DSSC; Photovoltaic performance; Graphene; Drop casting.

1. Introduction

Dye-sensitized solar cells (DSSCs) have attracted significant research interest as an alternative to silicon solar cell. DSSCs have low cost and relatively high power conversion efficiency (PCE) [1]. Traditionally, a DSSC uses a nanocrystalline titanium dioxide film coated with dye as the photoanode (PA), a Pt conductive glass as the counter electrode (CE), and an electrolyte containing an iodide/triiodide (I^-/I^{3-}) redox couple placed between the PA and CE. As a result, developing a novel customized material for the PA, CE, electrolyte, and dye to improve the DSSC's efficiency is important. The different parts of the DSSC each serve an important purpose in how it functions. The CE significantly impacts the overall performance of the DSSC as it collects electrons from the external circuit and passes them to the electrolyte by reducing triiodide I^{3-}.

Pt sufficiently fulfills the criteria for being a good CE material due to its very good electrical conductivity and electrocatalytic properties. However, Pt's high expense presents a concern for the commercial viability of DSSCs that could be mass produced, as the cost may be prohibitive [2].

Graphene (G) shows potential for various electronic [3] and optoelectronic applications [4] due to its high stability, flexibility, electrical conductivity, and specific surface area. Among carbonaceous materials, G is an attractive option. Its catalytic activity increases significantly when oxidized to form reduced graphene oxide (rGO) through oxidation and reduction processes, without vastly decreasing conductivity [5, 6]. A DSSC using a functionalized G-based CE achieved an efficiency of around 90% of a DSSC with a Pt-based CE [7]. Additionally, it was found that the FTO G Nano-platelet electrode was more catalytic than a Pt electrode for regenerating a Co-based redox couple [8]. Recent research from multiple groups has reported on rGO-based CE produced through thermal [9], chemical [10], electrochemical [11], and photo-thermal [12, 13] reduction of GO, which could be used for costly Pt CE free [14].

DSSCs are a significant technology in renewable energy due to their cost-effectiveness [15]. They use low-cost materials and simpler manufacturing processes, making them accessible for widespread use, especially in developing regions. Their flexibility allows for integration into various surfaces, including textiles and building materials [16]. Additionally, their lightweight nature makes them suitable for applications where traditional solar panels are impractical. DSSCs that incorporate graphene oxide (GO) and titanium dioxide (TiO_2) offer several advantages. GO improves the electrical conductivity of the photoanode and increases light absorption due to its high surface area. This facilitates better charge transport and reduces

*Corresponding author e-mail: doaa@eri.sci.eg; (Doaa M. Atia)

Received date 25 August 2024; revised date 20 September 2024; accepted date 02 October 2024

DOI: 10.21608/ejchem.2024.314249.10258

electron recombination, boosting efficiency [1, 17–19]. Moreover, a combination of TiO_2 and GO leverages their strengths, with TiO_2 providing excellent light-harvesting capabilities and GO enhancing charge transfer, resulting in improved power.
In [2], the authors described the synthesis of a novel Nano-hybrid material composed of nickel sulfide (NiS) on rGO CE by hydrothermal method, the obtained PCE was 9.5% and 78% FF.
In [20], a composite CE of GR Nano-sheets grafted with CoS was fabricated through a facile synthetic method where CoS Nano-particles were successfully grafted onto the surface of GR Nano-sheets. When used as the CE in a DSSC, a 7.28% power conversion efficiency (PCE) was reached.
In [21], the authors provided an overview of research examining the electrochemical and photovoltaic characteristics of GR-based CE materials, including GR, GR/Pt, GR combined with carbon materials, GR combined with conducting polymers, and GR combined with inorganic compounds. They summarized the design and advantages of each GR-based material configuration. The authors also suggested potential directions for developing new GR-based catalysts in future work further to enhance the performance and lower the cost of DSSCs.
The addition of rGO improves key aspects of the DSSC function. It decreases electron recombination by enhancing electrical conductivity, thus improving the PCE. The modified material also shows greater attraction to potential electron donors, making it more appealing. Transition metal sulfides like cobalt sulfide (Co_3S_4), cobalt mono-sulfide (CoS), molybdenum disulfide (MoS_2), and tin sulfide (SnS) demonstrate remarkable catalytic properties compared to platinum, along with ease of synthesis. This has driven significant interest in their application as CE materials [22].
The authors of [14] explored an alternative CE for DSSCs. The researchers fabricated a rGO electrode by applying a thick rGO paste onto an FTO substrate using the doctor-blade technique. This was followed by heat treatment at 500°C in an argon atmosphere.
While the rGO film's catalytic activity for (I^{3-}) reduction was lower than that of conventional Pt electrodes prepared by thermal decomposition, and the overall series resistance of the rGO-based cell was comparable to its Pt CE. In DSSC performance tests, the rGO electrode showed similar results to the Pt one. This suggested that rGO, a metal-free carbon material, could potentially replace Pt as a CE in DSSCs.
The work of [23] reported the preparation of GR and GR/SiO_2 films via drop-casting an FTO at room temperature without heat treatment as CE. The PCE of the DSSC achieved was 6.82% for a 2.5 μm thickness of GR/SiO_2.
Materials based on carbon, conducting polymers, transition metal oxides, nitrides, and sulfides have been investigated and shown promise as alternatives to Pt for CEs in DSSCs. Some of the options studied include composites of graphene or carbon with metal oxides, nitrides, or sulfides to leverage their synergistic effects on electrocatalytic activity and stability.
In [24] the authors aimed to synthesize GO using the Hummer method and rGO doped with CoS and CoMoS synthesized via a solvothermal method followed by heating to 200°C. The proposed thin film of rGO-CoMoS as a CE for DSSCs, achieving a Voc of 0.39 V, FF of 34.32%, and η of 1.54%.
In [25], flower-like cobalt molybdenum sulfide Nano-sheets intermixed with rGO ($Co_xMo_{(1-x)}S_2$/rGO) Nano-composite electrocatalysts were prepared using a facile one-step hydrothermal method and employed as the counter electrode in high-performance DSSCs.
The DSSC with CoS/rGO CE achieved a 7.08% PCE compared to the cell with Pt CE and much higher than the DSSC with CoS and GR CEs as in [26].
In DSSCs, the CEs play a crucial character in simplifying the electrochemical reactions, which are necessary for energy conversion. The performance of these electrodes significantly impacts the efficiency of DSSCs, as they directly influence the regeneration of the redox couple and the charge transfer. Developing effective counter and cost-effective electrodes remains a key focus in advancing DSSC technology.
G's 2-D single-atom-thick sheet structure gives graphene a high surface area-to-volume ratio and outstanding transport properties. G also generates little electrical noise and has uniquely superior electron transport efficiency due to its 2-D structure. In addition to these structural qualities, G displays outstanding chemical properties like very high electrical and thermal conductivity as well as strong optical absorption and mechanical strength. Overall, G's unique configuration results in unrivaled electrical, optical, and mechanical performance stemming from its unique chemical behaviors. These qualities indicate G's significant potential for a variety of technological applications. The exceptional properties of G make it an excellent material [27, 28].
G is the basic building block for all graphitic forms of carbon. It has a crystalline honeycomb lattice structure with carbon atoms arranged in a hexagonal sheet that is only one atom thick [29]. Its crystalline honeycomb lattice of sp2 hybridized carbon atoms provides outstanding electrical and thermal conductivity, strong optical absorption, and mechanical strength, making it ideal for various technological applications. However, graphene is hydrophobic due to the absence of oxygen groups [30].
Graphene oxide (GO) retains the 2-D structure of graphene but is oxidized, incorporating oxygen functional groups that improve its solubility in water and enable biomedical applications through further functionalization. Reduced graphene oxide (rGO) is an intermediate between graphene and GO, featuring a stable sp2 hybridized carbon structure with enhanced conductivity and chemically active sites, making it suitable for biomedical uses [28, 31, 32].
GO reduction can be achieved through thermal, chemical, and electrochemical methods, each resulting in different morphologies and electrical properties. Key design factors in GO reduction include the final C/O ratio, selectively removing specific oxygen group types (e.g. hydroxyl vs carboxyl vs epoxy), repairing surface defects from oxidation, using green reducing agents, and maintaining or improving desired physical and chemical properties of GO (mechanical strength, conductivity, optical properties, solubility/ dispersibility of nanosheets) [33, 34][35].

This work purposes to yield and analyze reduced graphene oxide (rGO) and its composite with cobalt sulfide (CoS) to improve their structural, optical, and electrical properties. The combination of rGO and Cobalt sulfide as a counter electrode material is an innovative method that utilizes the exclusive properties of these materials. This combination has the potential to knowingly recover the efficacy of DSSCs. Various characterization techniques, such as XRD and SEM analysis, as well as electrical property measurements, have been employed to gain a better understanding of the structural and functional attributes of the rGO and CoS composites.

This work aims to explore and improve the properties of graphene, graphene oxide (GO), and reduced sulfide-doped graphene (CoS/rGO) for various electronic technological applications. This involves researching methods to effectively reduce GO to achieve characteristics similar to pristine graphene, optimizing the carbon-to-oxygen ratio, selectively removing specific oxygen functional groups, and maintaining or enhancing the desired physical and chemical properties. Ultimately, the goal is to use the unique structural and functional characteristics of these materials to develop advanced applications in fields such as electronics, energy storage, and solar cells.

The paper is organized as follows: Section 2 provides the details of the experimental work, including the materials, preparation, and characterization of the CE and PA, as well as the measurement devices used. Section 3 discusses the results, focusing on the CE's structure, morphology, optical, and electrical properties. Finally, Section 4 presents the conclusion of the study.

2. Experimental work

The materials and solvents used in CE and PA preparation are presented in Table 1.

Table 1: The material used in the experimental work

No.	Materials	Chemical formula	Company
1	Cobalt nitrate hexahydrate	$Co(NO_3)_2.6H_2O$	Sigma Aldrich
2	Natural graphite flakes	C	Sigma-Aldrich
3	Sodium nitrate	$NaNO_3$	Kemiou Chemical Reagent Ltd., Tianjin
4	Potassium permanganate	$KMnO_4$	Merck
5	Sodium molybdate dehydrate	$Na_2MoO_4.2H_2O$	Sigma Aldrich
6	Thiourea	$CS(NH_2)_2$	Sigma Aldrich
7	Sulfuric acid, hydrochloric acid, ethylenediamine, hydrogen peroxide , and ethanol	H_2SO_4, HCl, $C_2H_8N_2$, H_2O_2, C_2H_5OH	Merck
8	Titanium isopropoxide	$Ti[OCH(CH_3)_2]_4$	Solaronix
9	Zirconium nitrate	$ZrO(NO_3)_2.xH_2O$	Solaronix
10	Electrolyte (iodide/triiodide)	I^-I^{3-}	ElNasr Pharmaceutical Chemical
11	N719 dye	Ruthenizer 535-bisTBA	Solaronix

The crystal structure of the promising sensitized thin films was analysed using an X-ray diffractometer (Bruker D8, Germany) with CuKα (λ = 1.54 Å) radiation in the 2θ range of 10-80°, operated at 40 kV and 40 mA. A scanning electron microscope (SEM, Hitachi S4800, Japan) was employed to examine the surface morphology of the synthesized thin films. Energy dispersive X-ray fluorescence spectrometry (EDXRF, Shimadzu EDX-7000) was used to determine the elemental composition and potential contaminants within the films. The optical properties of the films were assessed using a UV-VIS-NIR spectrophotometer (Shimadzu-2540) in the wavelength range of 300-1000 nm. A Keithley 4200 source-measure unit was utilized to measure the electrical resistance of the prepared thin films and to obtain the current density-voltage (J-V) characteristics of the DSSC.

2.1. Counter electrode preparation

Graphene oxide (GO) was created using the Hummers method [36, 37]. 5 grams of graphite and 2.5 grams of sodium nitrate were combined with sulfuric acid while stirring in an ice bath to keep the temperature below 20°C. Potassium permanganate was then slowly added to the mixture (Fig. 1).

Then, potassium permanganate is added gradually to the mixture. This step is crucial as it oxidizes the graphite, introducing oxygen-containing functional groups and converting it into graphene oxide. After removing the ice bath, the mixture was stirred at 40°C for 30 minutes. Deionized water was then slowly added to stop the reaction. An additional quantity of 30% hydrogen peroxide (H_2O_2) was slowly dropped into the solution using a dropper to terminate the reaction further. Hydrogen peroxide helps as a reducing agent that stops the oxidation reaction and transforms any leftover potassium permanganate into manganese sulfate. Extra deionized water was pipetted into the solution. Various techniques can be utilized for rGO, such as thermal annealing using microwave irradiation or photo-irradiation, as well as chemical reduction methods like solvothermal reduction, multi-step reduction, electrochemical reduction, and photochemical reduction [36, 38, 39].

This work uses thermal annealing to form a thin film of reduced graphene oxide (rGO) by heat-treating it to reduce the oxygen content. Glass substrates measuring 4 cm^2 were initially cleaned ultrasonic probe with soap solution, distilled water, and

acetone for 10 minutes each, then dried in air. The rGO film thickness was varied by drop casting different volumes (100, 200, 300, and 400 µL) of the graphene oxide suspension onto the substrates, which were then sintered at 400°C for 45 minutes in a muffle furnace. For the synthesis of the CoS/rGO composite, 50 mg of the GO suspension was sonicated in 100 mL of deionized water to form a stable suspension. Subsequently, 8.5 mmol of cobalt nitrate hexahydrate (Co $(NO_3)_2.6H_2O$) and 17 mmol of thiourea were dissolved into the graphene oxide suspension. This mixture is stirred for 2 hours, allowing the cobalt and sulfur to interact with the rGO. CoS/rGO films were synthesized by drop casting with 300 µL of CoS/rGO suspension onto a 4 cm^2 glass substrate. After drying, the films were annealed at 400 ^oC for 45 minutes in the furnace to obtain CoS/rGO CE. While the study proves the effectiveness of these materials under operational conditions remains uncertain. Future, the long-term stability of CoS/rGO composites, needs more studies to investigate the durability and performance degradation.

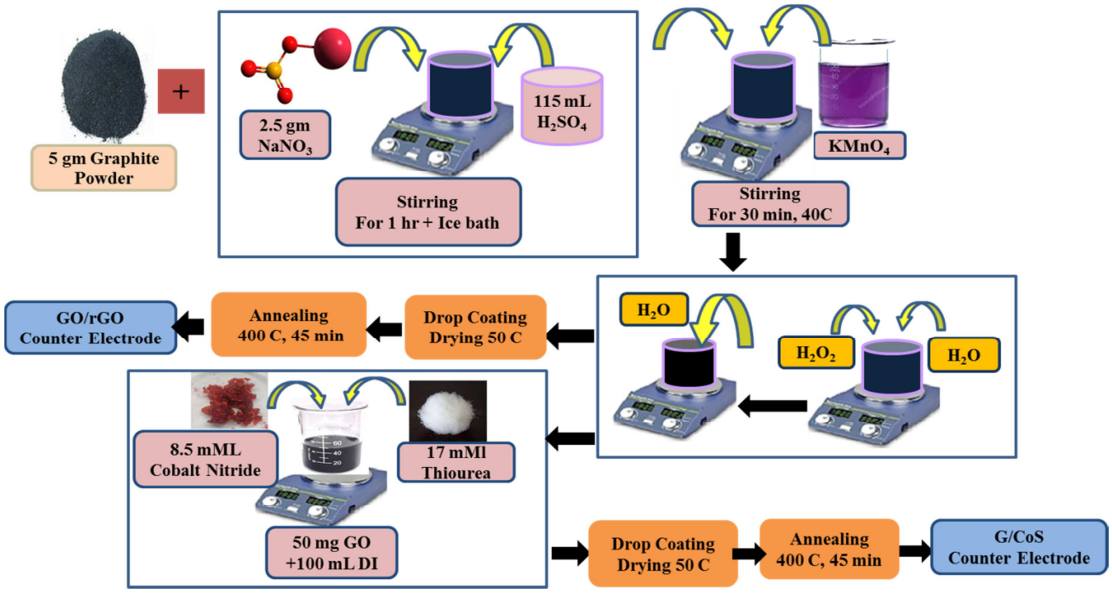

Figure 1: Experimental flowchart of the CoS/rGO counter electrode

2.2. Photo-anode preparation

We created Titinum-zirconiate (TZ) thin films using the sol-gel spin coating method on a glass substrate. To prepare the chemical solution of TiO_2, we dissolved Titanium Isopropoxide (Ti (OC_3H_7)) in methanol (CH_3OH) and isopropanol (2-propanol) ($(CH_3)_2CHOH$) as a solvent, and added citric acid (CH_3COOH) as a catalyst.

We obtained the TZ precursor by adding 2% Zirconia nitrate ($ZrO(NO_3)_2.xH_2O$) dissolved in citric acid and stirring the mixture at room temperature for 2 hrs. We coated all the films at 3000 rpm for 30 sec to form the TZ thin film. We repeated this step four times to achieve the desired thickness. After the deposition of each layer, the film was dried at 70°C for 5 minutes. Finally, the obtained films were annealed at 400°C for 1 hr.

2.3. Fabrication of DSSC

FTO is used as substrate instead of ordinary glass in coating of both photo-anode and CE. The photo-anode was sensitized by immersing it in a 29.7 mg dye solution (N719) containing 5 mL ethanol and 5 mL distilled water for 24 hrs at room temperature in the dark. Excess dye molecules were rinsed off with ethanol, and the electrode was dried in air. The dye-anchored photo-anode and CoS/rGO CE were assembled into a sealed sandwich-type cell. An iodide/triiodide redox electrolyte was prepared by dissolving 127 mg of iodine crystals and 830 mg of potassium iodate in 10 mL of ethanol under vigorous stirring for 30 minutes. The prepared electrolyte, being volatile, was covered with foil to prevent evaporation and left to equilibrate. The electrolyte was presented between the electrodes to fill the cell, and the device was sealed on two sides with tape.

3. Results and discussion

3.1. Structural characterization of the counter electrode

The crystal structures of the proposed samples, including 100 µL GO, 100 µL rGO, and 300 µL rGO, as well as 300 µL CoS/rGO, were determined by XRD, as illustrated in Fig. 2.

The XRD patterns were recorded in the 2θ range of 5–80°. At 2θ equal to 11° a sharp peak with high intensity confirms the formation of GO from natural graphite successfully. GO was then thermally reduced at 400 °C for 45 min to reduce GO and form rGO. The broad peak at 20^{o}-30^{o} in the three GO samples shown in Fig. 2 is slightly different. Whereby the 300 µL rGO sample exhibits a higher intensity, which indicates an increase in interlayer spacing.

A new broad peak (002) at ~2θ = 26° corresponding to an interlayer spacing of about 0.33 nm provides evidence for the reduction of GO and complete transformation to rGO. The XRD pattern of the CoS/rGO composite exhibits a (002) peak at 2θ = 25.2° with no additional peaks. The average crystallite size for the main peak was equal to 23.2 nm. The crystallite size was calculated using Scherrer's Equation [40]:

$$D = \frac{(0.9\,\lambda)}{(\beta\cos\theta)} \quad (1)$$

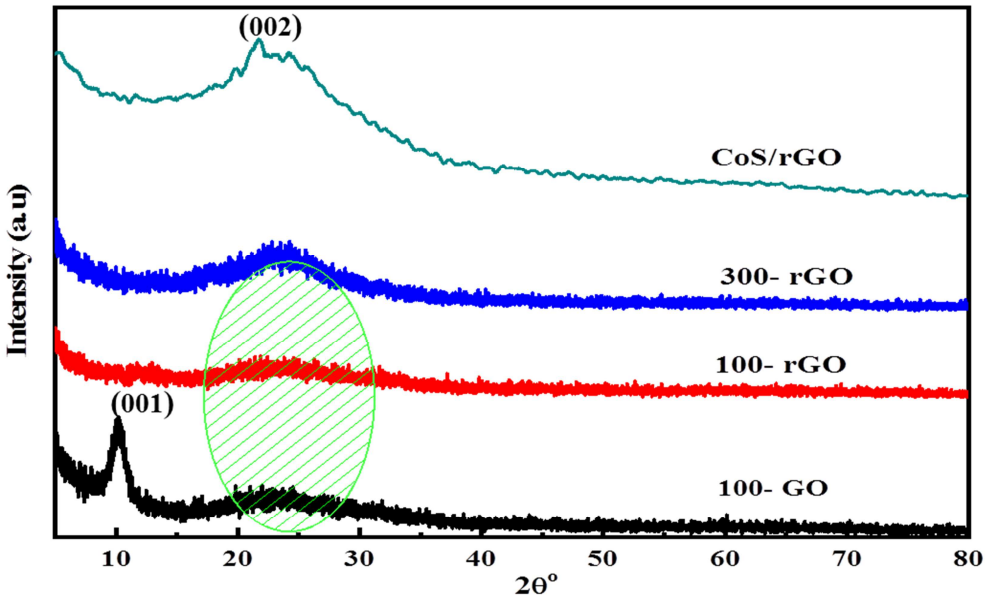

Figure 2: XRD characterizations of 100 µL GO, 100 µL rGO, 300 µL rGO, and 300 µL CoS_2/ rGO samples

3.2. Morphological Properties

The surface morphologies of the synthesized rGO and CoS/rGO were dissected using SEM as illustrated in Fig 3(a, b). The two sample images exhibited a wrinkled structure due to the rapid removal of O_2-containing functional groups in rGO. Typical SEM images of 300 µL rGO and 300 µL CoS/ rGO appear as 2D nanosheet morphologies with folded textures with rough surfaces and irregular edges. The two samples give grain sizes 193 nm and 270 nm.

The elemental compositions of the rGO and CoS/rGO samples were obtained from the samples' EDX. Figure 3 (c, d) displays the EDX patterns of rGO and CoS/rGO thin films. The rGO and CoS/rGO primarily consist of carbon and oxygen, with other elements on the glass substrate in addition to Co and S elements in CoS/rGO sample. Table 2 summarizes the chemical compositions of rGO and CoS/rGO. Figure 3(d) gives the EDX spectrum of the CoS/rGO sample, confirming the presence of Co, S, C, and O elements.

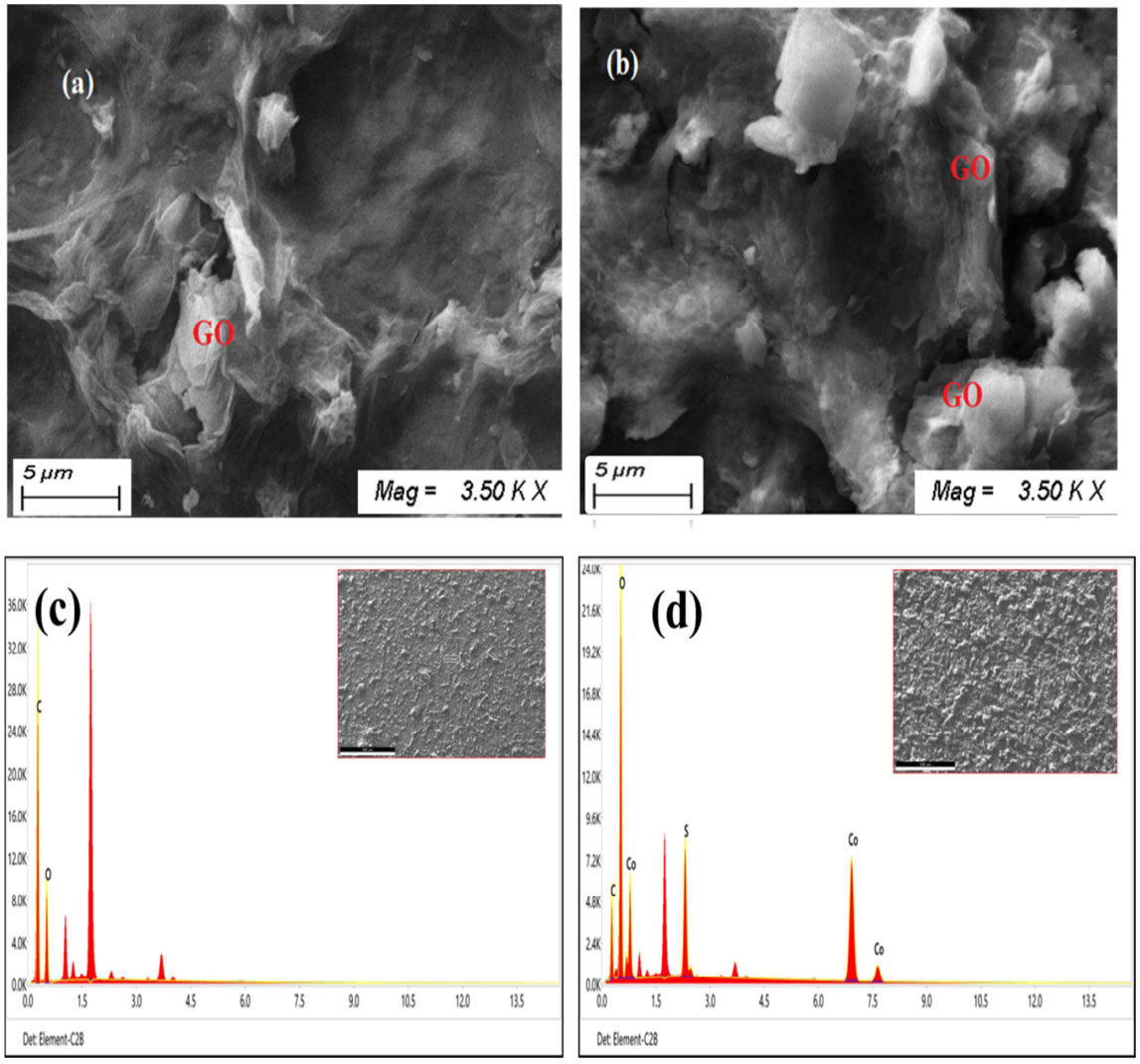

Figure 3: Morphology of CE thin film (a) SEM images of 300 µL rGO, (b) SEM images of 300 µL CoS/ rGO, (c) EDX of 300 µL rGO, (d) EDX of 300 µL CoS/rGO

3.3. Transmission electron microscopy results

More detailed morphological and structural information on GO is obtained using TEM analysis. Figure 4 demonstrates the TEM analysis of GO and CoS/rGO. The samples possess a spherical nanoparticle structure. The prepared samples showed free voids, cracks, slight particle aggregation, and non-uniform distribution on the substrate surface. The TEM image shows the GO nanoparticles are scattered irregularly, with diameters ranging from 14.3-60.4 nm and an average of 30.46 nm. The TEM image of the CoS/rGO composite shows the nanoparticles are also scattered irregularly, with diameters ranging from 15.5-103 nm and an average of 32.28 nm.

Table 2: The EDX elemental analysis of rGO and CoS/rGO

Elements atomic (%)	Carbon C	Oxygen O	Co	S	C/O
100 µL rGO	62.88	37.12	-	-	1.69
300 µL rGO	69.19	30.81	-	-	2.24
300 µL CoS/rGO	36.75	52.89	6.98	3.41	0.69

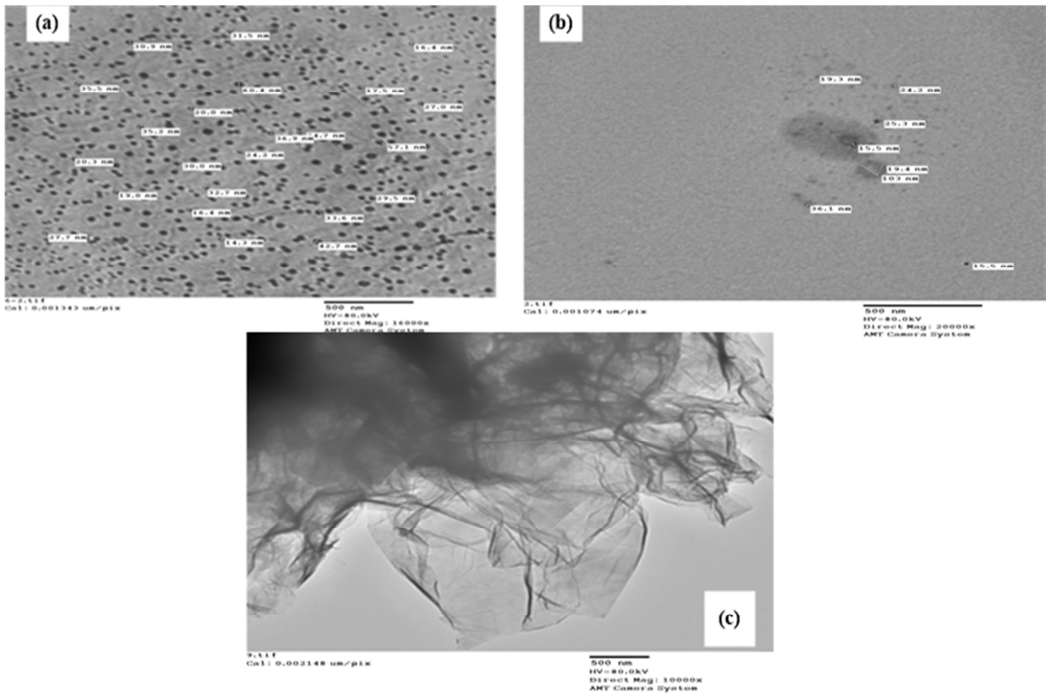

Figure 4: TEM image of (a) GO, (b) CoS/GO at 20000x direct magnification, and (c) CoS/GO at 10000x direct magnification

3.4. Optical properties

Figure 5 (a) displays the transmittance of rGO and CoS/rGO samples as a function of photon energy. It illustrates that the films have low transmittance over the photon energy range due to the high thickness of the prepared films and CoS/rGO Nano-composite transmittance is higher than that of rGO.

The absorption coefficient (α) of rGO and CoS/rGO could be determined by the following equation [40] :

$$\alpha = \frac{\ln(1/T)}{d} \quad (2)$$

Where T and d are the layer transmission and thickness, respectively. The absorbance in the range of 1.25 eV to 4.25 eV proposes that these structures have a broad absorption spectrum, permitting them to efficiently absorb a wide range of photon energies (Fig. 5 (b)). The absorbance range in the graph indicates two distinct peaks: one for reduced graphene oxide (rGO) at around 280 nm and another for the CoS/rGO composite at 286 nm (Fig. 5(b)). The peak at 280 nm for rGO is owing to its electronic transitions, which are inclined by its assembly and the existence of functional groups. The peak at 286 nm corresponds to the CoS/rGO composite and may arise from the combined effects of both the rGO and the cobalt sulfide (CoS) components [41].

This distinctive is mainly advantageous for many applications such as photodetectors, solar cells, and other optoelectronic devices.

Figure 5 (c) represents the dependency of the extinction coefficient (K) on the photon energy of rGO and CoS/rGO samples. The K has decreased with photon energy increment. The weedy interaction between the photons and electrons in the proposed films led to small value of the k. The k of the rGO and CoS/rGO samples have been calculated by using the following relationship [42][43]:

$$K = \frac{\alpha\lambda}{4\pi} \quad (3)$$

The light speed in the films represents the refractive index (n). The n can be calculated by [42][43]:

$$n = \frac{1+R}{1-R} + \sqrt{\frac{4R}{(1-R)^2} - K^2} \quad (4)$$

Figure 5 (d) shows the decrement of refractive index (n) with photon energy. By adjusting the photon energy, it's possible to create a specific material for producing electro-optic and optoelectronic devices. The Tauc relation was used to evaluate the energy band gap of rGO and CoS/rGO film as [44] [45]:

$$(\alpha h\vartheta)^2 = A(h\vartheta - E_g) \quad (5)$$

Where α is the absorption coefficient, ϑ is the frequency of light radiation, h is Planck's constant, A is a constant, and E_g is band gap energy. Figure 5 (e) represented the tangent loss variation. Figure 5 (f) presents the corresponding Tauc plot, $(\alpha h\vartheta)^2$ with $h\vartheta$, of the rGO and CoS/rGO thin film. The E_g was estimated by determining the x-intercept of an extrapolated Tauc plot. The E_g of rGO is approximately 3.252 eV and decreased to 3.05 eV for CoS/rGO thin film. The reduced E_g for the CoS/rGO thin film expands its absorption range into the visible region of the electromagnetic spectrum, thereby enhancing its light harvesting efficiency. The diminished E_g in CoS/rGO compared to rGO may increase conductivity and improve optical properties. The optical conductivity was calculated using the absorption coefficient (α) in the following equation [42]:

$$\sigma_{opt} = \frac{\alpha nc}{4\pi} \tag{6}$$

$$\sigma_{elect} = \frac{2\lambda\sigma_{opt}}{\alpha} \tag{7}$$

In Figure 5 (g and h), the electrical conductivity (σ_{elect}) and the optical conductivity (σ_{opt}) change with the photon energy for both rGO and CoS/rGO films. These samples show a high photon response in the rGO and CoS/rGO samples. This issue is due to the carriers' transformation to conduction from the valance band in the rGO and CoS/rGO.

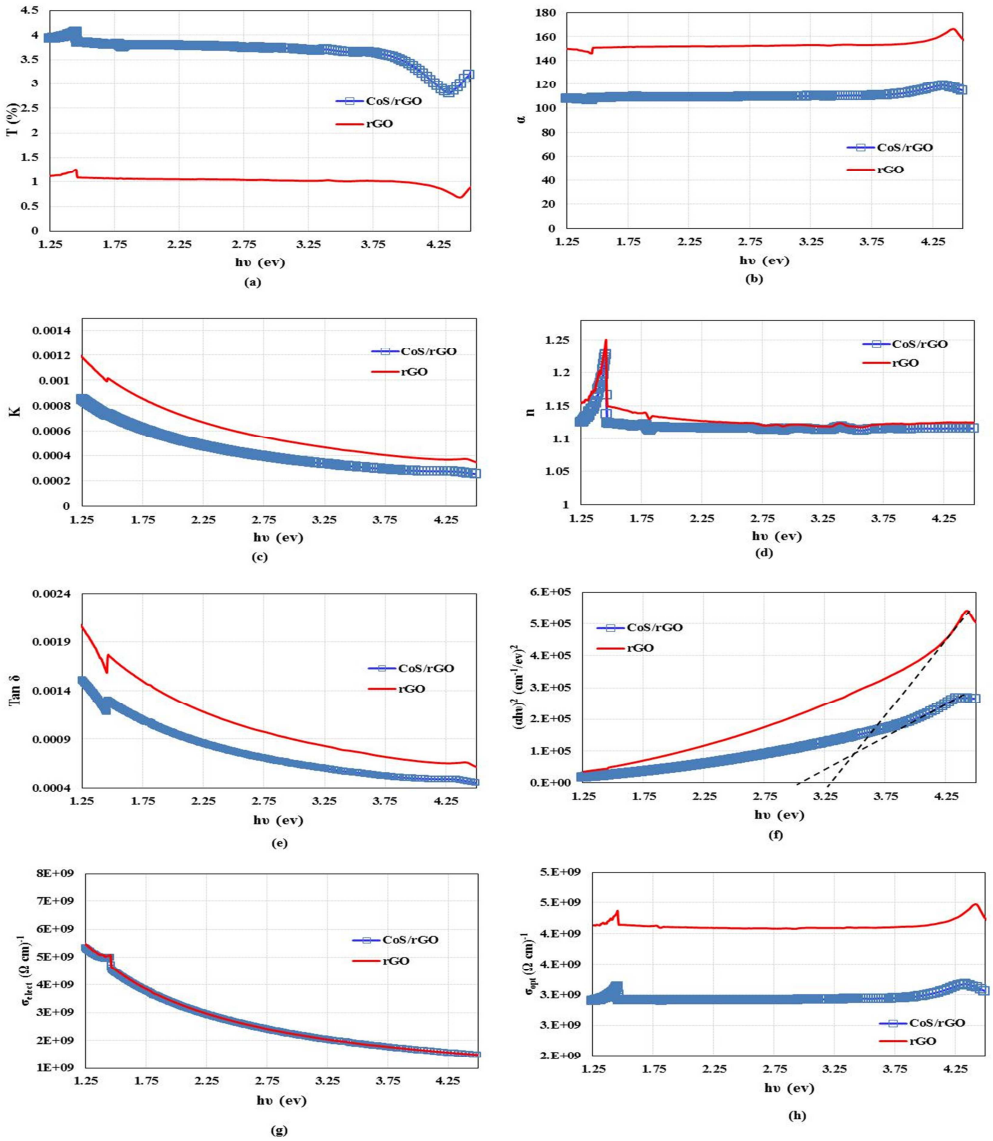

Figure 5: The rGO and CoS/rGO thin films' optical properties

3.5. Electrical properties

The rGO thin film also exhibits a low sheet resistance (R_{sh}) compared to GO due to more O_2 functional groups in graphene oxide. The R_{sh} of the rGO sample with different volumes (100, 200, 300, and 400 µL) was carried out using a four-point prob. Table 3 shows the variation of the R_{sh} with the GO amount used to prepare rGO films. Here, for the optimization of the GO amount, the sintering temperature and time were kept fixed at 400 ◦C and 45 min. The sample 300 µL GO showed the lowest value of R_{sh}. The R_{sh} of rGO thin film was 3.6 kΩ/cm2 for 100 µL, 0.7 kΩ/cm^2 for 300 µL, and 1.5 kΩ/cm^2 for 400 µL. The result obtained is of the same order of magnitude as that reported in the literature. Thick rGO films often consist of multiple rGO domains. Grain boundaries can scatter charge carriers, leading to increased resistance. Thicker rGO films can lead to interlayer coupling and changes in electronic band structure, which can impede carrier mobility. Defects introduced during the growth process can trap charge carriers, increasing resistance. At higher thicknesses, there may be more scattering events due to phonons and impurities, which can reduce mobility and increase resistance. Heating can alter the electronic properties of rGO; higher temperatures can lead to increased scattering, thus raising resistance. These factors combined can lead to higher sheet resistance in thick rGO films compared to thinner films or monolayer rGO.

Finally, the R_{sh} of the selected thickness doped with CoS; 300 µL CoS/rGO was measured to be 37.5Ω which showed a decreasing R_{sh} due to adding CoS in the GO.

Table 3: Sheet resistance of CE thin film

Solution volume (µL)	Sheet Resistance
100 µL GO	3.6 kΩ/cm^2
100 µL rGO	2.2kΩ/cm^2
300 µL rGO	0.7kΩ/cm^2
400 µL rGO	1.5kΩ/cm^2
300 µL CoS/rGO	37.5 Ω/cm^2

3.6. Photovoltaic performance

The CoS/rGO electrode served as the CE to achieve high-efficiency DSSC. Figure 6 compares the J-V curves of DSSC based on the CoS/rGO proposed CE and Pt reference electrode. The corresponding PV parameters, such as V_{oc}, J_{sc}, FF and η are 0.75 V, 17.88 mA/cm^2, 0.527, and 7.0759%, respectively. The detailed electrical parameters of the proposed DSSC are summarized in Table 4.

As a reference solar cell, the Pt-based DSSC has a high V_{oc} of 0.78 V, J_{sc} of 12.8445 mA/cm^2, FF of 0.5164, and a PCE of 5.1744% under 100 mW/cm^2. The high performance of the DSSC with the CoS/rGO CE has been attributed to the high conductivity of the material. The high conductivity accelerates the electron transfer process from the CE to the electrolyte. It also increases the regeneration of electrons within the electrolyte and dye, thereby improving the performance of the DSSC. Several factors can affect the FF of DSSC, High series resistance can occur due to poor contact between layers, The absorption spectrum and stability of the dye can impact the amount of light absorbed and subsequently influence FF. The ionic conductivity and viscosity of the electrolyte can affect the speed of charge transport. High rates of electron-hole recombination occurred. Poor surface morphology of the thin films can lead to defects and increased recombination. The fill factor can vary with different light intensities; under low light, FF may decrease due to increased relative impact of resistive losses. The design and layering of the DSSC can influence charge transport and collection, affecting the fill factor.

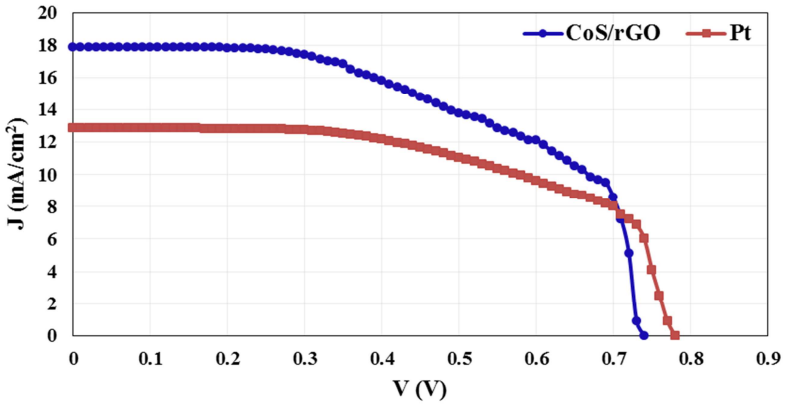

Figure 6: The CoS/rGO and Pt CE-based DSSC J-V characteristics

Table 4: DSSC electrical parameters at 100 mW/cm^2

CE	J_{SC} (mA/cm^2)	V_{oc}(mV)	FF	η (%)
Pt	12.8445	0.78	0.516	5.1744
CoS/ rGO	17.8886	0.75	0.527	7.0759

4. Conclusion

This study aimed to propose an effective and low-cost combination of counter electrode (CE) for dye-sensitized solar cells (DSSCs). The modified Hummers method was employed to prepare graphene oxide (GO). Our results showed that thicker reduced graphene oxide (rGO) films exhibited higher sheet resistance compared to thinner films. This was primarily due to increased scattering events from phonons and impurities, as well as thermal effects at elevated temperatures. A nanocomposite film of cobalt sulfide (CoS) and rGO as the CE for a DSSC was prepared using a simple one-pot and low-temperature drop-casting method. The CoS/rGO-based DSSC demonstrated an acceptable efficiency of 7.0759% under 1000 W/m^2. The synergistic effects of CoS and graphene show great promise as a viable alternative for Pt-free DSSC devices, representing a significant advance in efficient and sustainable solar energy conversion. The incorporation of CoS into the rGO matrix significantly reduced the sheet resistance (R_{sh}), with a measured value of 37.5 for the 300 μL CoS/rGO sample, indicating enhanced conductivity and improved performance as a counter electrode in dye-sensitized solar cells. In-situ prepared CoS/rGO CEs were suitable for high-efficiency Pt-free DSSCs, resulting in an economic impact and simplicity of the preparation process. For future research, we will focus on assessing the strength of cobalt sulfide/reduced graphene oxide composites in practical conditions. Also, works on evolving the synthesis method and testing the performance of the composite in different environmental conditions to guarantee scalability.

5. Conflict of interest

There is no conflict of interest.

6. References

1. Alsaati SAA, Abdoon RS, Hussein EH, et al (2024) Unveiling the potential of graphene and S-doped graphene nanostructures for toxic gas sensing and solar sensitizer cell devices: insights from DFT calculations. J Mol Model 30:1–15. https://doi.org/10.1007/S00894-024-05994-1/METRICS
2. Sarkar A, Chakraborty AK, Bera S (2018) NiS / rGO nanohybrid : An excellent counter electrode for dye sensitized solar cell. Solar Energy Materials and Solar Cells 182:314–320. https://doi.org/10.1016/j.solmat.2018.03.026
3. Houk Jang, Yong Ju Park, Xiang Chen, Tanmoy Das, Min-Seok Kim J-HA (2016) Graphene-Based Flexible and Stretchable Electronics.pdf. Advanced Materials 28:4184–4202
4. Wei J, Zang Z, Zhang Y, et al (2017) Enhanced performance of light-controlled conductive switching in hybrid cuprous oxide/reduced graphene oxide (Cu2O/rGO) nanocomposites. Optics Letters 42:911–914
5. Huang D, Zhang B, Zhang Y, et al (2013) Electrochemically reduced graphene oxide multilayer films as metal-free electrocatalysts for oxygen reduction. J Mater Chem A Mater 1:1415–1420. https://doi.org/10.1039/c2ta00552b
6. Gao R, Hu N, Yang Z, et al (2013) Paper-like graphene-Ag composite films with enhanced mechanical and electrical properties. Nanoscale Res Lett 8:2–9. https://doi.org/10.1186/1556-276x-8-32
7. Roy-Mayhew JD, Bozym DJ, Punckt C, Aksay IA (2010) Functionalized graphene as a catalytic counter electrode in dye-sensitized solar cells. ACS Nano 4:6203–6211. https://doi.org/10.1021/nn1016428
8. Kavan L, Yum J-H, Grätzel M (2011) Graphene nanoplatelets outperforming platinum as the electrocatalyst in co-bipyridine-mediated dye-sensitized solar cells. Nano Letters 11:5501–5506. https://doi.org/10.1021/nl203329c
9. Jang HS, Yun JM, Kim DY, et al (2012) Moderately reduced graphene oxide as transparent counter electrodes for dye-sensitized solar cells. Electrochimica Acta 81:301–307. https://doi.org/10.1016/j.electacta.2012.07.021
10. Zheng H, Neo CY, Mei X, et al (2012) Reduced graphene oxide films fabricated by gel coating and their application as platinum-free counter electrodes of highly efficient iodide/triiodide dye-sensitized solar cells. Journal of Materials Chemistry 22:14465–14474. https://doi.org/10.1039/c2jm30612c
11. Xu X, Huang D, Cao K, et al (2013) Electrochemically reduced graphene oxide multilayer films as efficient counter electrode for dye-sensitized solar cells. Scientific Reports 3:. https://doi.org/10.1038/srep01489
12. Nagavolu C, Susmitha K, Raghavender M, et al (2016) Pt-free spray coated reduced graphene oxide counter electrodes for dye sensitized solar cells. Solar Energy 137:143–147. https://doi.org/10.1016/j.solener.2016.08.002
13. Yeh M-H, Lin L-Y, Chang L-Y, et al (2014) Dye-sensitized solar cells with reduced graphene oxide as the counter electrode prepared by a green photothermal reduction process. ChemPhysChem 15:1175–1181. https://doi.org/10.1002/cphc.201301128
14. Sarker S, Lee K, Woo H, et al (2017) Reduced graphene oxide for Pt-free counter electrodes of dye-sensitized solar cells. Solar Energy 158:42–48. https://doi.org/10.1016/j.solener.2017.09.029
15. Sasikumar R, Thirumalaisamy S, Kim B, Hwang B (2024) Dye-sensitized solar cells: Insights and research divergence towards alternatives. Renewable and Sustainable Energy Reviews 199:114549. https://doi.org/10.1016/J.RSER.2024.114549

16. Omar A, Ali MS, Abd Rahim N (2020) Electron transport properties analysis of titanium dioxide dye-sensitized solar cells (TiO2-DSSCs) based natural dyes using electrochemical impedance spectroscopy concept: A review. Solar Energy 207:1088–1121. https://doi.org/10.1016/J.SOLENER.2020.07.028
17. El Nahrawy AM, Abou Hammad AB, Mansour AM (2021) Structural investigation and optical properties of Fe, Al, Si, and Cu–ZnTiO 3 nanocrystals. Phys Scr 96:115801. https://doi.org/10.1088/1402-4896/ac119e
18. Habibi Jetani G, Rahmani MB (2020) TiO2/GO nanocomposites: synthesis, characterization, and DSSC application. The European Physical Journal Plus 2020 135:9 135:1–21. https://doi.org/10.1140/EPJP/S13360-020-00739-4
19. Yasin A, Guo F, Demopoulos GP (2016) Aqueous, Screen-Printable Paste for Fabrication of Mesoporous Composite Anatase-Rutile TiO2 Nanoparticle Thin Films for (Photo)electrochemical Devices. ACS Sustain Chem Eng 4:2173–2181. https://doi.org/10.1021/ACSSUSCHEMENG.5B01625/SUPPL_FILE/SC5B01625_SI_001.PDF
20. Rahman MU, Xie F, Li Y, et al (2019) Grafting cobalt sulfide on graphene nanosheets as a counterelectrode for dye-sensitized solar cells. Journal of Alloys and Compounds 808:151701. https://doi.org/10.1016/J.JALLCOM.2019.151701
21. Lu M, Chang C, Wei T, Lin J (2016) Recent Development of Graphene-Based Cathode Materials for Dye-Sensitized Solar Cells. 2016:
22. Abinaya S, Sakthivel R, Ramachandran K, et al (2024) Design and fabrication of NiCo2S4@rGO as an efficient Pt free triiodide reducing agent for dye-sensitized solar cell application. Chemical Physics Impact 100676. https://doi.org/10.1016/J.CHPHI.2024.100676
23. Gong F, Li Z, Wang H, Wang Z (2012) Enhanced electrocatalytic performance of graphene via incorporation of SiO 2 nanoparticles for dye-sensitized solar cells †. https://doi.org/10.1039/c2jm33483f
24. Sathishkumar M, Manikandan M Thin layer of nano nomposite RGO COMOS as a counter electrode on Dye Sensitized Solar Cell (DSSC) Thin layer of nano nomposite RGO COMOS as a counter electrode on Dye Sensitized Solar Cell (DSSC). 4–11. https://doi.org/10.1088/1742-6596/2190/1/012044
25. Senthilkumar R, Ramakrishnan S, Balu M, et al (2023) CoxMo(1−x)S2 intermixed reduced graphene oxide as efficient counter electrode materials for high-performance dye-sensitized solar cells. International Journal of Hydrogen Energy 48:5901–5914. https://doi.org/10.1016/J.IJHYDENE.2022.11.156
26. Wang G, Zhang J, Kuang S, et al (2014) The production of cobalt sulfide/graphene composite for use as a low-cost counter-electrode material in dye-sensitized solar cells. Journal of Power Sources 269:473–478. https://doi.org/10.1016/J.JPOWSOUR.2014.07.018
27. Abed HH, Al-Aaraji NAH, Salman JM, et al (2022) Theoretical study on dye-sensitized solar cells using graphene quantum dot and curcumin, pahthalocyanine dyes. IOP Conf Ser Earth Environ Sci 1088:. https://doi.org/10.1088/1755-1315/1088/1/012012
28. Madlool HA, Salman JM, Yosif AA, et al (2022) Comparative Adsorption Calculations for Carbon Mono-Oxide and Hydro Cyanide Gas Molecules Interaction with Graphene Material Using Density Function Theory. Egypt J Chem 65:385–391. https://doi.org/10.21608/EJCHEM.2022.120895.5420
29. Yang G, Li L, Lee WB, Ng MC (2018) Structure of graphene and its disorders: a review. Science and Technology of Advanced Materials 19:613–648. https://doi.org/10.1080/14686996.2018.1494493
30. Kaur H, Garg R, Singh S, et al (2022) Progress and challenges of graphene and its congeners for biomedical applications. Journal of Molecular Liquids 368:120703. https://doi.org/10.1016/J.MOLLIQ.2022.120703
31. Yan D, Liu J, Zhang Z, et al (2021) Dual-functional graphene oxide-based nanomaterial for enhancing the passive and active corrosion protection of epoxy coating. Compos B Eng 222:109075. https://doi.org/10.1016/J.COMPOSITESB.2021.109075
32. Bao J, Liu Y-H, Guo - B, et al (2022) Theoretical study on dye-sensitized solar cells using graphene quantum dot and curcumin, pahthalocyanine dyes. IOP Conf Ser Earth Environ Sci 1088:012012. https://doi.org/10.1088/1755-1315/1088/1/012012
33. De Silva KKH, Huang HH, Joshi RK, Yoshimura M (2017) Chemical reduction of graphene oxide using green reductants. Carbon N Y 119:190–199. https://doi.org/10.1016/J.CARBON.2017.04.025
34. Stankovich S, Dikin DA, Piner RD, et al (2007) Synthesis of graphene-based nanosheets via chemical reduction of exfoliated graphite oxide. Carbon N Y 45:1558–1565. https://doi.org/10.1016/J.CARBON.2007.02.034
35. Smith AT, LaChance AM, Zeng S, et al (2019) Synthesis, properties, and applications of graphene oxide/reduced graphene oxide and their nanocomposites. Nano Materials Science 1:31–47. https://doi.org/10.1016/J.NANOMS.2019.02.004
36. Mohamedy MH, Sayed MM, Ahmed NM, Zahran MB (2020) High power capability of mos2 based aqueous electrolyte supercapacitor. International Journal of Nanoelectronics and Materials 13:547–564
37. Zaaba NI, Foo KL, Hashim U, et al (2017) Synthesis of Graphene Oxide using Modified Hummers Method: Solvent Influence. Procedia Eng 184:469–477. https://doi.org/10.1016/j.proeng.2017.04.118
38. Gordani GR, Loghman Estarki MR, Kiani E, Torkian S (2022) The effects of strontium ferrite micro-and nanoparticles on the microstructure, phase, magnetic properties, and electromagnetic waves absorption of graphene oxide-SrFe12O19-SiC aerogel nanocomposite. J Magn Magn Mater 545:168667. https://doi.org/10.1016/J.JMMM.2021.168667
39. Gordani GR, Loghman Estarki MR, Danesh M, et al (2022) Microstructure, phase, magnetic properties, and electromagnetic wave absorption of graphene oxide – Ni0.7Zn0.3Fe2O4 – Al2O3 aerogel. Ceram Int 48:3059–3069. https://doi.org/10.1016/J.CERAMINT.2021.10.081
40. Toraya MM, Atia DM, Nahrawy AM El, et al (2022) Synthesis and Characterization of Cu-Incorporated Zinc Tin Zorcinate Thin Film as a Promising Candidate as Absorber Layer in DSSC. Egypt J Chem 65:663–675. https://doi.org/10.21608/ejchem.2021.87118.4214

41. Emiru TF, Ayele DW (2017) Controlled synthesis, characterization and reduction of graphene oxide: A convenient method for large scale production. Egyptian Journal of Basic and Applied Sciences 4:74–79. https://doi.org/10.1016/J.EJBAS.2016.11.002
42. Toraya MM, Atia DM, El Nahrawy AM, et al (2022) Sol gel synthesis and characterization of porous nanosized oxide 70TiO2-30 MgO film for anode solar cell application. International Journal of Nanoelectronics and Materials 15:353–366
43. M. Toraya M, M. El Nahrawy A, M.Mansour A, et al (2022) Impact of Cu concentration on the properties of sol-gel spin-coated Cu-ZnZrSnO thin films : evaluation of Ag / Cu-ZrZnSn / p-Si / Al Schottky diodes. Silicon 14:10837–10847
44. El-Nahrawy, A, Ali, A. Abou Hammad, A. Youssef A (2016) Influences of Ag-NPs doping chitosan/calcium silicate nanocomposites for optical and antibacterial activity. Int J Biol Macromol. https://doi.org/10.1016/j.ijbiomac.2016.08.045
45. Caglar Y, Caglar M, Ilican S (2012) Microstructural, optical and electrical studies on sol gel derived ZnO and ZnO : Al films. Current Applied Physics 12:963–968. https://doi.org/10.1016/j.cap.2011.12.017